An ex vivo experiment to reproduce a forward fall leading to fractured and non-fractured radii

Edison Zapata, Frédéric Rongieras, Jean-Baptiste Pialat, Hélène Follet, David Mitton

ZAPATA, Edison, RONGIERAS, Frédéric, PIALAT, Jean-Baptiste, FOLLET, Hélène, MITTON, David, 2017, An ex vivo experiment to reproduce a forward fall leading to fractured and non-fractured radii, Journal of Biomechanics, Elsevier, DOI: 10.1016/j.jbiomech.2017.08.013

An *ex vivo* experiment to reproduce a forward fall leading to fractured and non-fractured radii

E. Zapata[1,2], F. Rongieras[1,4], J-B Pialat[2,3], H. Follet[2], D. Mitton[1]

[1] Univ Lyon, Université Claude Bernard Lyon 1, IFSTTAR, LBMC UMR_T9406, F69622, Lyon, France

[2] Univ Lyon, Université Claude Bernard Lyon 1, INSERM, Lyos UMR1033, F69622, Lyon, France

[3] Service de Radiologie, Centre Hospitalier Lyon Sud, Pierre-Bénite, France

[4] Service de chirurgie orthopédique et traumatologique – Hôpital d'instruction des armées Desgenettes - 69003 Lyon, France

***Corresponding author**:*

David Mitton

LBMC

Site Ifsttar Lyon-Bron

25 Avenue François Mitterrand

69675 BRON FRANCE

Phone: +33 4 72 14 23 61,

E-mail address: david.mitton@ifsttar.fr

Keywords: Fall, Bone strength, Fracture, Radius, Biomechanics

Word count: 1993

Abstract

Forward falls represent a risk of injury for the elderly. The risk is increased in elderly persons with bone diseases, such as osteoporosis. However, half of the patients with fracture were not considered at risk based on bone density measurement (current clinical technique). We assume that loading conditions are of high importance and should be considered. Real loading conditions in a fall can reach a loading speed of 2 m/s on average. The current study aimed to apply more realistic loading conditions that simulate a forward fall on the radius *ex vivo*. Thirty radii from elderly donors (79 y.o. ± 12 y.o., 15 males, 15 females) were loaded at 2 m/s using a servo-hydraulic testing machine to mimic impact that corresponds to a fall. Among the 30 radii, 14 had a fracture after the impact, leading to two groups (fractured and non-fractured). Surfacic strain fields were measured using stereovision and allow for visualization of fracture patterns. The average maximum load was 2963 ± 1274 N. These experimental data will be useful for assessing the predictive capability of fracture risk prediction methods such as finite element models.

1. Introduction

Among the different bone fractures, those of the distal section of the radius occur earlier in life than other osteoporotic fractures and can be interpreted as a warning signal for later, more deleterious fractures (L. J. Melton et al., 2010). The gold standard method for clinical diagnosis of osteoporosis and evaluation of the risk for fracture is Dual X-ray Absorptiometry (DXA) (World Health Organization, 2004). It has been shown, however, that this measurement presents insufficient sensitivity, and indeed 50 % of fractures occur in patients considered as non-osteoporotic (Siris et al., 2004).

Ongoing research has proposed different methods to improve sensitivity. One of these methods is analysis by micro-finite element models (µFEM) based on High Resolution peripheral Quantitative Computed Tomography (HR-pQCT) (Pistoia et al., 2002, Vilayphiou et al., 2011). All validation studies have shown that bone strength is better estimated by µFEM (R^2 between 0.73 and 0.92) than by DXA measurements (R^2 between 0.31 and 0.71) (van Rietbergen and Ito, 2015). Despite this good level of prediction of bone strength using µFEM, retrospective studies have not yet provided clear evidence that the output of µFEM provides better predictors of fracture risk than DXA measurements (van Rietbergen and Ito, 2015).

Currently, the assessment of bone fragility using HR-pQCT implies a finite element analysis under static axial loading (Pistoia et al., 2002) (Macneil and Boyd, 2008) (Varga et al., 2009) (Hosseini et al., 2017). However, only 15 % of fall cases are associated with an axial load on the radius (L J Melton et al., 2010) and asymmetrical body orientation influences loading of the radius (Burkhart,TA et al., 2017). The most common angle between the floor and the arm found in the forward fall is 75° (Greenwald et al., 1998) (Chiu and Robinovitch, 1998) and the average velocity when the subject hits the floor can reach 2 m/s (Tan et al., 2006) (Troy and Grabiner,

2007). Thus, we assume that this dynamic loading should be considered for *ex vivo* experiments that result in fractured and non-fractured bones. Having these two groups in known loading conditions would be of interest to assess new methodologies to predict bone fracture risk.

Previous studies loaded radii until failure in all cases, with some under quasi-static conditions (Pistoia et al., 2002) (Macneil and Boyd, 2008) (Varga et al., 2009) (Hosseini et al., 2017) and one using fall conditions (Burkhart et al., 2012). In this context, the aim of this study is to propose an *ex vivo* experiment to reproduce a forward fall loading condition, leading to fractured and non-fractured radii.

2. Methods

Thirty radii from elderly donors (50 to 96 y.o., 79± 12 y.o., 15 males, 15 females) were considered. The bones were provided by the Departement Universitaire d'Anatomie Rockefeller (Lyon, France) through the French program on voluntary corpse donation to science. First, during the dissection, 2/3 of the distal radius was cut and cleaned of soft tissues. Each radius was wrapped in a saline-moistened gauze and frozen at -20° C before the experiments.

The day before the experiments, bones were thawed for 16 hours at 4°C and then 6 hours at room temperature. The third part of the distal radius was exposed after being potted in a polyurethane resin (reference: 84A&B, Esprit Composite, Paris, France) in a steel cylinder (Figure 1. Using a positioning laser, radii were potted with an alignment of 75° between the anterior face of the radius and the ground, without any tilt in any other planes. This position reproduces alignment of the radius in the most common forward fall (Chiu and Robinovitch, 1998).

Taking into account that the scaphoid and lunate are both involved in the mechanism of fracture of the distal radius (Jupiter and Fernandez, 1997), a rigid polyurethane mold was made to reproduce a simplification of these bones for each radius.

A silicon rubber kept the mold on the radius, but also allowed some displacement (a few millimeters) in perpendicular directions to the impact, as expected in real life.

The pot was placed in a horizontal cylinder bar on a rail system, which was free to slide along the loading axis (Figure2). This bar had a weight of 12.5 kg, which was an arbitrary value representing the mass involved in a fall, i.e., a percentage of body weight. This weight was the same for all the tests. The rail system allows one to limit the loading on the radius to avoid having bone fracture in all cases.

The radius was then loaded through the mold at 2 m/s using a hydraulic high-speed testing machine (LF technologies, France). At the beginning of the test, the distance between the impactor and the mold was 50 mm. This distance allowed the acceleration of the impactor and stabilization of its speed to reach 2 m/s before impact. From there, the displacement of the stroke was set to 10 mm. A six-axis sensor (105515TF, Humanetics, Germany) was tightened onto the impactor. Velocities and positions were also obtained by instrumentation systems of the testing machine. Accelerations were obtained by adding an external accelerometer to the impact plate.

The data from the experiment was analyzed in order to obtain the reaction load curve over time and to retrieve the maximum load during the test. The treatment of this curve consisted of filtering and subtraction of inertial load (caused by the inertia of the moving mass). For the filtering, we used frequency analysis (Fast Fourier transform) to evaluate the spectrum of frequencies making part of the signal. A Butterworth frequency filter was chosen to process this

signal. The low peak attenuation frequency was set to 300 Hz and the high peak attenuation coefficient was set to 5000 Hz.

Four high-speed cameras (FASTCAM SA3, Photron, Japan) recorded the impact. Two cameras were placed facing the ulnar face of the radius, and recorded the test using a 105 mm F2.8 DG Macro sigma lenses. The other two cameras were placed facing the anterior face of the radius, and recorded the test using a 50 mm Z1.4/50 mm ZF planar Zeiss lens. The cameras were set to record with a resolution of 1024 x 1024 pixels at 2000 images per second, using a shutter speed of 50 µs. The radii were illuminated using three projectors (400D, Dedolight, Germany). Bone fracture was assessed by using the high-speed recordings, but also by a radiologist who interpreted radiographs after the impact. Colles' fractures featured radial shortening. Barton's fractures presented a dislocation of the volar rim of the radius.

Video recordings were analyzed using VIC3D stereo-correlation software (Correlated Solution, South Carolina, USA). A speckle was painted on the specimen (Figure 2B) to compute 3D surface strain fields (von Mises strains).

Radii were measured by Dual X-Ray absorptiometry to obtain bone mineral density values (g/cm^2) and status (Osteoporotic, Osteopenia and Normal) based on T-score (BMDCS/Hologic curves) (Table 1).

3. Results

3.1 Maximum loads from the experiment

Maximum loads are shown in Table 1 and correspond to the failure loads for the fractured cases. Fractures were not consistently associated with the largest loads and depended on bone strength. Stronger bones can indeed sustain larger loads before breaking.

3.2 Fracture cases and type of fracture

Among the 30 radii, 14 had a fracture after impact, and 16 did not fracture. In three cases over the 14 fracture cases the radius were not classified as osteoporotic according to DXA measurements.

The type of fracture is indicated in Table 1. The prevalent fracture types are Colles' and Barton's. The main fracture types are shown in Figure 3. Colles' fractures were stable, and the fracture was barely visible by a simple overview of the bone. In this experiment for the Barton's fractures, the movement of the volar rim causes opening of the radius into two main parts along its longitudinal axis.

There were also two cases of complex fractures, for example having several fractures propagating simultaneously from different directions. However, the displacement pattern noted was mainly volar and radial.

3.3 Strain analysis

Fractures were associated with two types of strain patterns corresponding to Colles' fractures and Barton's fractures. For the strongest bone, von Mises strain reached a maximum value of 0.9% on the anterior region and 2% on the ulnar side. For the weakest bone, the maximum measured von Mises strain value before fracture was 1.5% on the anterior region, and 3.1% on the ulnar side.

Examples of surface strains for the anterior region are shown in Figure 4. This figure shows strain concentration in the fracture region.

4. Discussion

This study provided experimental data reproducing a forward fall on the radius leading to fractured and non-fractured bones.

The average values of the experimental peak loads in the current study: 2963 (1274) N are in agreement with those reported in the literature: 2142 (1229) N (Burkhart et al., 2014). When observing the high-speed videos, it was found that among the 30 radii, some of them presented a sliding effect of the mold over the articular surface. This effect could be related to the fact that during a forward fall over the forearm, the scaphoid and lunate move partially in the plane perpendicular to the longitudinal axis of the radius (Belloti et al., 2013). As a consequence, a radius with a titled articular surface may not fracture, not because its strength is high, but because the loading was lowered due to the joint shape.

Regarding strain analysis, the highest strain was found at the ulnar side, as observed in a previous study (Burkhart et al., 2014). Apart from qualitative observations of the strain pattern during the loading, the strain field will be used in future studies to compare experimental fracture patterns revealed by strain distributions and strains computed from numerical models.

The loading conditions will be reproduced in models according to experimental studies. Maximal loads and strain fields will be compared to experimental data to assess model predictions. A failure criterion will be defined and the fracture prediction of the model will be compared to fractures observed experimentally.

The main limitations of the current study are related to positioning and the rigidity of the articular molds. Their initial positions might be slightly different from an optimal position (congruence with joint surface of the radius) even if the molds are maintained in position using a piece of silicon rubber as illustrated Figure 2B. Subject-specific molds were used to spread loading onto the joint surface and a choice was made to not glue them onto the joint surface to better reproduce the potential sliding of the joint during loading. Articular molds were composed of a polyurethane resin and present rigidity close to that of the radius. The influence of mold rigidity will have to be taken into account for further modelling of the boundary conditions of this experiment. Moreover, the load was spread on the entire joint surface which is different from a real-life situation. This condition was chosen in the experiment to control boundary conditions for further consideration in a numerical model.

Another limitation is related to the use of cadaveric samples. Similar to most *ex vivo* studies on bones, the specimens were frozen, which is considered as the best conservation mode. Soft tissues were removed to obtain well-defined boundary conditions to be considered in the future models.

Finally, the same load was applied onto the radii despite the body weight of a subject. A unique weight was considered to obtain fractured and non-fractured radii at the end of the experiments.

5. Conclusions

Thirty radii were tested under dynamic non-axial loading to reproduce a forward fall configuration. Most previous studies have evaluated bone strength of the radius under static conditions and until failure in all cases. The originality of the current study is related to the two

groups of bones (fractured and non-fractured). Having these two groups with known loading conditions is of great interest to assess the predictive capability of finite element models and to check whether consideration of dynamic non-axial loading of the radius in those models could improve fracture risk assessment.

Acknowledgements

The authors would like to acknowledge Leila Ben Boubaker for her assistance during the experiments, Jean-Paul Roux, Yves Caire and Stéphane Ardizzone for their technical support. This work was done in the framework of LabEx PRIMES (ANR-11-LABX-0063).

Conflict of interest statement

There is no conflict of interest for any of the authors.

References

Belloti, J.C., Santos, J.B.G. dos, Erazo, J.P., Iani, L.J., Tamaoki, M.J.S., Moraes, V.Y. de, Faloppa, F., 2013. A new method for classifying distal radius fracture: the IDEAL classification. Rev. Bras. Ortop. Engl. Ed. 48, 36–40. doi:10.1016/j.rboe.2012.06.002

Burkhart, T.A., Andrews, Dunning, C.E., 2012. Failure characteristics of the isolated distal radius in response to dynamic impact loading. J. Orthop. Res. 30, 885–892. doi:10.1002/jor.22009

Burkhart, Quenneville, C.E., Dunning, C.E., Andrews, D.M., 2014. Development and validation of a distal radius finite element model to simulate impact loading indicative of a forward fall. Proc. Inst. Mech. Eng. [H]. doi:10.1177/0954411914522781

Burkhart,TA, Brydges E, Stefanczyk J, Andrews DM, 2017. The effect of asymmetrical body orientation during simulated forward falls on the distal upper extremity impact response of healthy people. J Electromyogr Kinesiol 33:48-56.

Chiu, J., Robinovitch, S.N., 1998. Prediction of upper extremity impact forces during falls on the outstretched hand. J. Biomech. 31, 1169–76.

Greenwald, R.M., Janes, P.C., Swanson, S.C., McDonald, T.R., 1998. Dynamic impact response of human cadaveric forearms using a wrist brace. Am. J. Sports Med. 26, 825–830.

Hosseini, H.S., Dünki, A., Fabech, J., Stauber, M., Vilayphiou, N., Pahr, D., Pretterklieber, M., Wandel, J., Rietbergen, B. van, Zysset, P.K., 2017. Fast estimation of Colles' fracture load of the distal section of the radius by homogenized finite element analysis based on HR-pQCT. Bone 97, 65–75. doi:10.1016/j.bone.2017.01.003

Jupiter, J.B., Fernandez, D.L., 1997. Clinical Perspective Comparative Classification for Fractures of the Distal End of the Radius.

Macneil, J. a, Boyd, S.K., 2008. Bone strength at the distal radius can be estimated from high-resolution peripheral quantitative computed tomography and the finite element method. Bone 42, 1203–13. doi:10.1016/j.bone.2008.01.017

Melton, L.J., Christen, D., Riggs, B.L., Achenbach, S.J., Müller, R., Van Lenthe, G.H., Amin, S., Atkinson, E.J., Khosla, S., 2010. Assessing forearm fracture risk in postmenopausal women. Osteoporos. Int. 21, 1161–1169. doi:10.1007/s00198-009-1047-2

Melton, L.J., Christen, D., Riggs, B.L., Achenbach, S.J., Müller, R., van Lenthe, G.H., Amin, S., Atkinson, E.J., Khosla, S., 2010. Assessing forearm fracture risk in postmenopausal women. Osteoporos. Int. J. Establ. Result Coop. Eur. Found. Osteoporos. Natl. Osteoporos. Found. USA 21, 1161–9. doi:10.1007/s00198-009-1047-2

Pistoia, W., van Rietbergen, B., Lochmüller, E.-M., Lill, C. a, Eckstein, F., Rüegsegger, P., 2002. Estimation of distal radius failure load with micro-finite element analysis models based on three-dimensional peripheral quantitative computed tomography images. Bone 30, 842–8.

Siris, E.S., Chen, Y.-T., Abbott, T.A., Barrett-Connor, E., Miller, P.D., Wehren, L.E., Berger, M.L., 2004. Bone Mineral Density Thresholds for Pharmacological Intervention to Prevent Fractures. Arch. Intern. Med. 164, 1108–1112. doi:10.1001/archinte.164.10.1108

Tan, J.-S., Eng, J.J., Robinovitch, S.N., Warnick, B., 2006. Wrist impact velocities are smaller in forward falls than backward falls from standing. J. Biomech. 39, 1804–11. doi:10.1016/j.jbiomech.2005.05.016

Troy, K.L., Grabiner, M.D., 2007. Asymmetrical ground impact of the hands after a trip-induced fall: experimental kinematics and kinetics. Clin. Biomech. Bristol Avon 22, 1088–95. doi:10.1016/j.clinbiomech.2007.07.014

van Rietbergen, B., Ito, K., 2015. A survey of micro-finite element analysis for clinical assessment of bone strength: The first decade. J. Biomech., In Memory of Rik Huiskes 48, 832–841. doi:10.1016/j.jbiomech.2014.12.024

Varga, P., Baumbach, S., Pahr, D., Zysset, P.K., 2009. Validation of an anatomy specific finite element model of Colles' fracture. J. Biomech. 42, 1726–31. doi:10.1016/j.jbiomech.2009.04.017

Vilayphiou, N., Boutroy, S., Szulc, P., Van Rietbergen, B., Munoz, F., Delmas, P.D., Chapurlat, R., 2011. Finite element analysis performed on radius and tibia HR-pQCT images and fragility fractures at all sites in postmenopausal women. J. Bone Miner. Res. 26, 965–973. doi:10.1002/jbmr.297

World Health Organization, 2004. Who scientific group on the assessment of osteoporosis at primary health care level (No. May 2004).

Figure and table legends

Figure 1: Construction of the articular mold. A. Modelling clay shell is put on the distal radius to contain the resin. B. Polyurethane resin inside the modelling clay shell. C. After removal of the modelling clay.

Figure 2: A. Diagram of the experiment. This configuration loads the radius at 75° with a velocity of 2m/s, representing the forward fall case studied. B. Final setup of the experiment.

Figure 3: Main type of fracture found in the experiments. A. Colles' fracture (radial shortening). B. Barton fracture (volar). C. complex fracture.

Figure 4: von Mises strain distribution in the anterior region, for (A) the strongest and (B) the weakest bone. A) Non-Fractured radius at the maximum load. B) Fractured radius (Colles' type fracture). First frame after fracture (the red part of the strain pattern is equal to or above 2%).

Table 1: Experimental data (age, sex, maximal load, type of fracture, ultra-distal (UD) bone area, Bone Mineral Density, T-score, category).

273 Figure 1

274

275

276

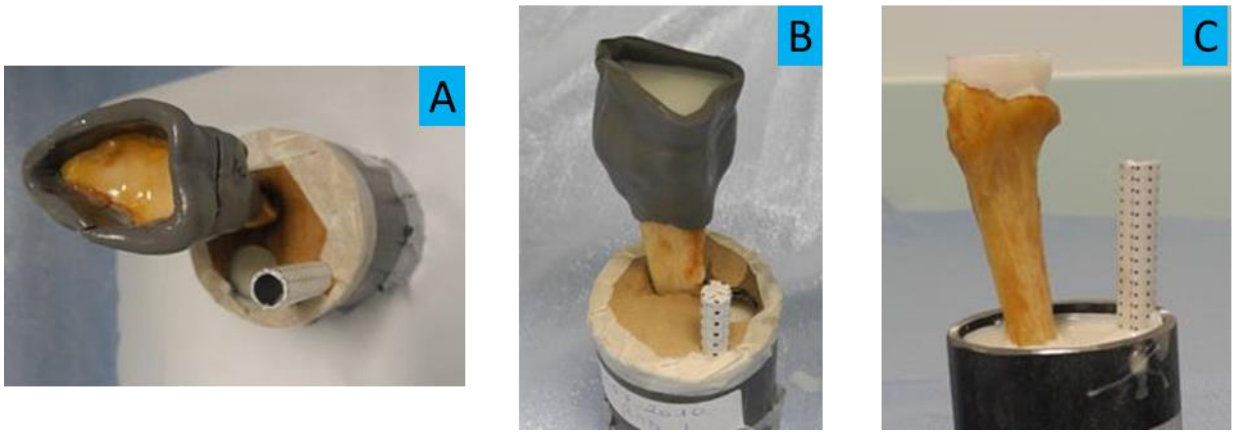

277

278

279

280 Figure 2

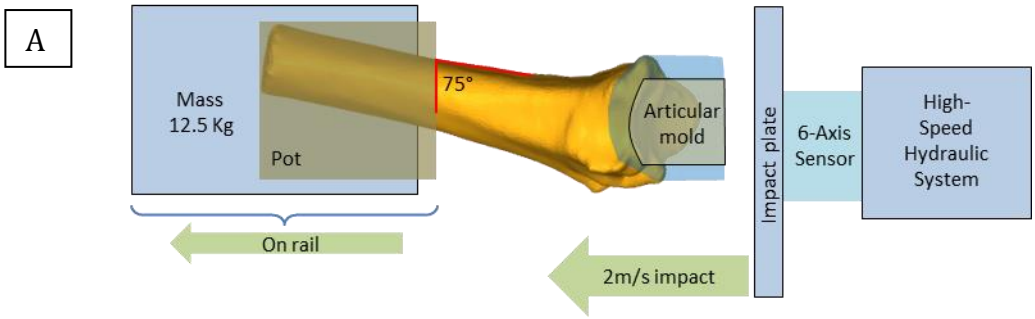

281

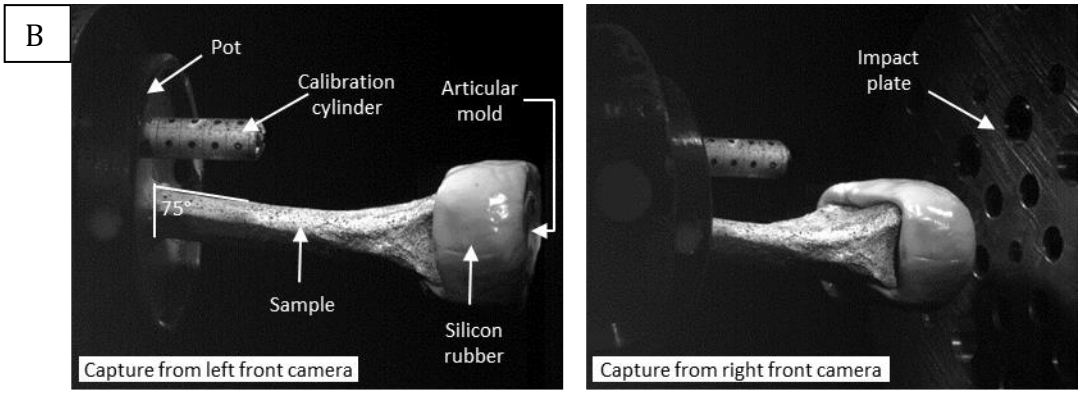

282

283

284 Figure 3

285 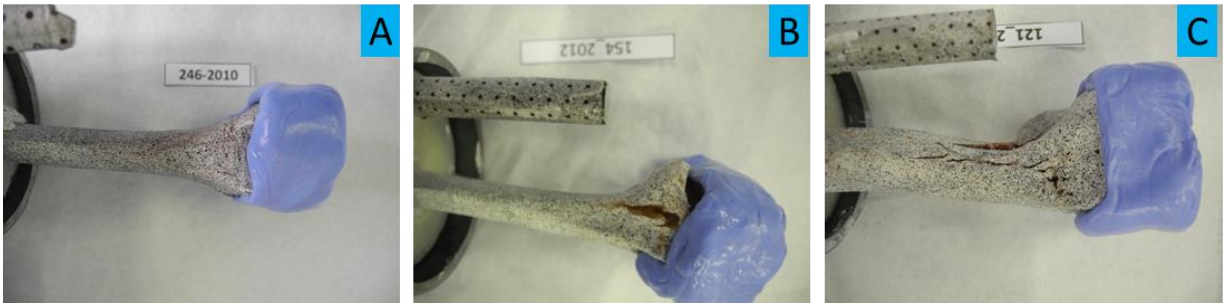

286

287 Figure 4

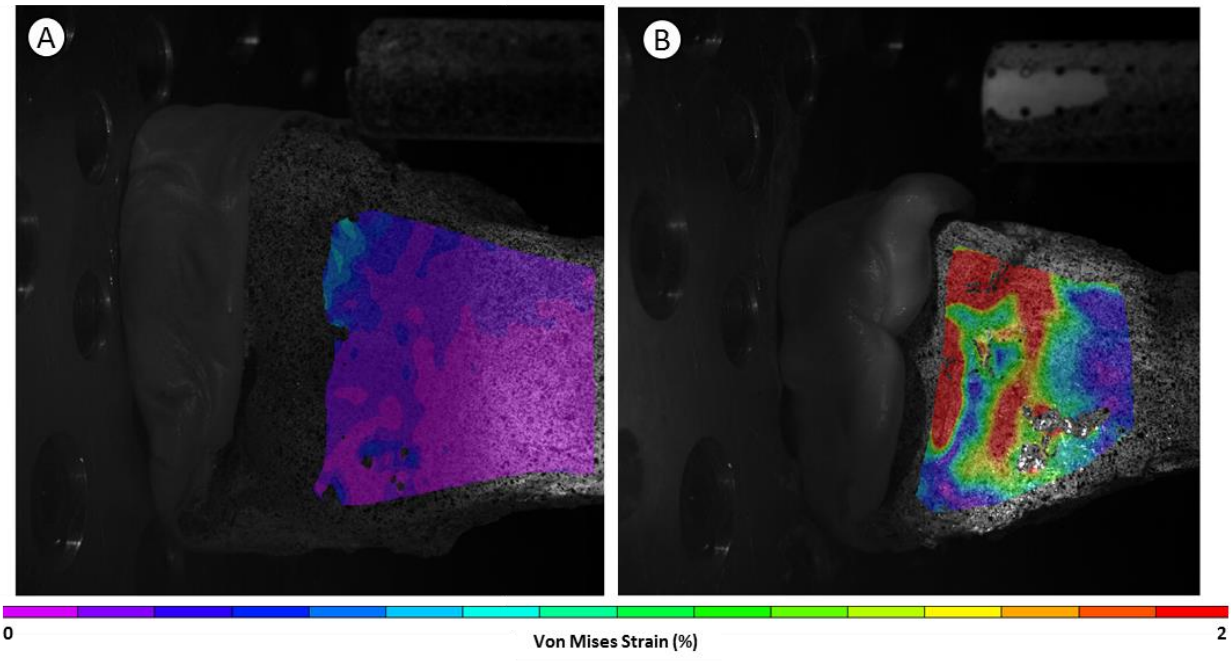

288

289

290 Table 1

Age	Sex	Maximum load (N)	Fractured	Type of Fracture	UD bone area (cm^2)	Bone Mineral Density (BMD, g/cm^2)	T SCORE UD	Category
95	F	1176	Yes	Colles	3,31	0,16	-4,96	Osteoporotic
74	F	849	Yes	Proximal	3,70	0,19	-4,42	Osteoporotic
88	F	1777	Yes	Proximal	3,81	0,21	-3,97	Osteoporotic
73	F	1625	Yes	Colles	3,47	0,22	-3,77	Osteoporotic
96	F	2182	Yes	Barton	3,87	0,25	-3,25	Osteoporotic
98	F	1692	No		3,52	0,28	-2,80	Osteoporotic
87	F	2055	Yes	Complex	3,57	0,28	-2,77	Osteoporotic
91	F	2697	No		3,32	0,29	-2,70	Osteoporotic
86	F	2634	Yes	Barton	4,06	0,30	-2,52	Osteoporotic
85	F	1629	Yes	Colles	3,63	0,30	-2,52	Osteoporotic
57	F	1965	Yes	Colles	3,58	0,30	-2,51	Osteoporotic
95	F	2381	Yes	Barton	3,88	0,38	-1,07	Osteopenia
50	F	3925	No		3,15	0,41	-0,57	Normal
56	F	2478	No		3,57	0,41	-0,53	Normal
76	F	3486	No		3,63	0,41	-0,53	Normal
66	M	2927	Yes	Complex	4,39	0,32	-3,78	Osteoporotic
65	M	2971	Yes	Colles	3,69	0,34	-3,47	Osteoporotic
94	M	2936	No		4,61	0,40	-2,54	Osteoporotic
74	M	4203	No		3,77	0,40	-2,40	Osteopenia
76	M	2206	No		4,25	0,41	-2,37	Osteopenia
77	M	3674	No		4,24	0,42	-2,12	Osteopenia
89	M	3990	No		4,24	0,44	-1,85	Osteopenia
79	M	5818	No		4,87	0,44	-1,81	Osteopenia
88	M	6265	No		4,70	0,44	-1,77	Osteopenia
75	M	4178	No		4,35	0,44	-1,76	Osteopenia
67	M	4344	No		4,35	0,44	-1,74	Osteopenia
83	M	3825	Yes	Barton	3,99	0,48	-1,14	Osteopenia
79	M	2178	No		4,61	0,50	-0,85	Normal
80	M	2903	Yes	Barton	4,08	0,50	-0,72	Normal
80	M	3929	No		4,70	0,52	-0,42	Normal
79		2963			3.96	0.36	-2.25	Mean
12		1274			0.47	0.10	1.22	Standard deviation

291

292